Available online at www.sciencedirect.com
ScienceDirect
Physica D 227 (2007) 70–77
PHYSICA D
www.elsevier.com/locate/physd

Bifurcation structure of dissipative solitons

Damià Gomila*, A.J. Scroggie, W.J. Firth

Department of Physics, University of Strathclyde, 107 Rottenrow East, Glasgow, G4 0NG, United Kingdom

Received 31 October 2005; received in revised form 14 October 2006; accepted 11 December 2006
Available online 23 December 2006
Communicated by J. Lega

Abstract

In this paper we analyze in detail the structure of the phase space of a reversible dynamical system describing the stationary solutions of a model for a nonlinear optical cavity. We compare our results with the general picture described in [P.D. Woods, A.R. Champneys, Physica D 129 (1999) 147; P. Coullet, C. Riera, C. Tresser, Phys. Rev. Lett. 84 (2000) 3069] and find that the stable and unstable manifolds of homogeneous and patterned solutions present a much higher level of complexity than predicted, including the existence of additional localized solutions and fronts. This extra complexity arises due to homoclinic and heteroclinic intersections of the invariant manifolds of low-amplitude periodic solutions, and to the fact that these periodic solutions together with the high-amplitude ones constitute a one-parameter family generating a closed line on the symmetry plane.

Keywords: Homoclinic bifurcations; Localized structures; Dissipative solitons; Reversible systems; Dynamical systems

1. Introduction

Dissipative spatial localized structures, also known as dissipative solitons (DS), appear in a large variety of physical systems, such as granular media, chemical reactions, gas discharges and fluids [1]. In nonlinear optical cavities they appear due to the interplay between diffraction, nonlinearity, driving and dissipation, and are known as cavity solitons. Cavity solitons are interesting not only from a theoretical point of view, but also for their potential applications in optoelectronic devices [2,3].

A mathematical description of the bifurcation sequence of a general class of DS including cavity solitons was recently given in Refs. [4–6]. The existence of DS is related to a situation in which a stable infinite pattern coexists with a stable homogeneous solution. There one can envisage a configuration in which there is a domain of pattern and a homogeneous domain, with a front connecting both solutions. In general one or other solution will dominate, so that the front will move until the entire space is filled with the dominant state. One might expect a point in parameter space at which the dominant role switches from the pattern to the homogeneous state. In fact, this "point" spreads out in parameter space into a "locking range" of finite width, within which the front is stationary i.e. the two states can stably coexist [7]. Using generic properties of ordinary differential equations, one can show that such a locking range is generally accompanied by an infinite sequence of localized patterns (close-packed clusters of DS) [5] as well as their counterparts (clusters of holes) in the pattern solution [6]. This scenario is one of the possible results of the unfolding of a codimension-2 degenerate Hamiltonian–Hopf bifurcation [4].

In this paper we analyze in detail the structure of the phase space that yields DS in the four-dimensional dynamical system that describes the stationary solutions of a specific nonlinear optical system: a ring cavity filled with a self-focusing Kerr medium [8,9]. We find that the stable and unstable manifolds of homogeneous and pattern solutions, on whose form and relative position the results reported in [4–6] rely, present a much higher level of complexity than predicted, including the existence of additional localized solutions and complexes. This extra complexity arises due to homoclinic and heteroclinic intersections of the stable and unstable manifolds of the high and low-amplitude periodic solutions, corresponding to the stable and unstable patterns of the full PDE respectively,

* Corresponding address: Institut Mediterrani d'Estudis Avançats, IMEDEA (CSIC-UIB), Ed. Mateu Orfila Campus Universitat Illes Balears, 07122 Palma de Mallorca, Spain. Tel.: +34 971 172 668; fax: +34 971 173 248.
E-mail address: damia@imedea.uib.es (D. Gomila).

0167-2789/$ - see front matter © 2006 Elsevier B.V. All rights reserved.
doi:10.1016/j.physd.2006.12.008

and to the fact that these periodic solutions constitute a one-parameter family generating a closed, rather than open, line on the symmetry plane. This also induces additional heteroclinic intersections between the invariant manifolds of the homogeneous state and low-amplitude periodic orbits. Associated with these intersections are new fronts and localized states. In order to demonstrate the generality of our results we show that the same phenomenology is present in a different optical system: a cavity with a saturable absorber [10].

The paper is organized as follows: In Section 2 we summarize the picture presented in [4–6], analyze the Kerr cavity model and compare our results with the general theory. In Section 3 we reproduce the main results found in the Kerr cavity for a saturable absorber cavity, showing the generality of the phenomena. Finally, in Section 4 we give some concluding remarks.

2. Kerr cavity

As a representative model system, we consider an optical cavity filled with a nonlinear self-focusing Kerr medium and driven by a plane-wave pump. In the mean field approximation, and with one transverse spatial dimension, the dynamics of the slowly varying amplitude of the electric field $E(x,t)$ can be described by [8]:

$$\partial_t E = -(1+\mathrm{i}\theta)E + \mathrm{i}\partial_x^2 E + E_0 + \mathrm{i}|E|^2 E, \tag{1}$$

where θ is the detuning between the frequency of the input pump and the nearest cavity resonance, and E_0 is the amplitude of the pump. The homogeneous steady state solution $E_s = u_s + \mathrm{i}v_s$ is given implicitly by

$$E_s = E_0/[1+\mathrm{i}(\theta - I_s)], \tag{2}$$

where $I_s = |E_s|^2$.

Eq. (2) has a unique solution for $\theta < \sqrt{3}$. Here we restrict ourselves to this range, and use I_s and θ as convenient control parameters. The homogeneous solution is stable for $I_s < 1$ and becomes modulationally unstable at $I_s = 1$ with critical wavenumber $k_c = \sqrt{2-\theta}$, leading to the formation of a stripe pattern.

Above threshold there is a finite band of unstable wavenumbers associated with a one-parameter family of pattern solutions. For $\theta > 41/30$ the transition is subcritical [8,9], so that stable homogeneous and patterned solutions co-exist for intensities $I_s < 1$, below the modulational instability.

In addition, however, there is a coexistent *unstable* family of low amplitude patterns spanning the same wavenumber range, whose relevance will become clear in the following.

The point ($I_s = 1$, $\theta = 41/30$) signals the codimension-2 Hamiltonian–Hopf bifurcation analyzed in [4]. Associated with this subcritical bifurcation are localized states. In this context, localized states with a single main peak are known as cavity solitons [2], while multiple-peak structures can be regarded, in some sense, as bound states of cavity solitons. These states can be considered as regions of a pattern sitting on a background of the homogeneous solution.

Setting $\partial_t E = 0$ in Eq. (1) yields the condition for a stationary solution. The resulting complex, second order ordinary differential equation can be recast as a four dimensional dynamical system in the variables

$$\mathbf{V} \equiv [a = d_x \mathrm{Re}(E), b = d_x \mathrm{Im}(E), u = \mathrm{Re}(E), v = \mathrm{Im}(E)]^{\mathrm{T}}.$$

Moreover, this system is reversible [4–6] with respect to the involution $\mathcal{R}$:

$$\mathcal{R}\begin{bmatrix} a \\ b \\ u \\ v \end{bmatrix} = \begin{bmatrix} -a \\ -b \\ u \\ v \end{bmatrix} \tag{3}$$

so that $\mathcal{R}\mathbf{V}(-x) = \mathbf{V}(x)$. The symmetry plane Π is defined as the set of points invariant under $\mathcal{R}$, in our case obviously defined by $a = b = 0$. Orbits (including fixed points) closed under the action of $\mathcal{R}$ are termed reversible, and all such orbits intersect Π. In particular, the homogeneous solution E_s (which corresponds to a fixed point) and the set P of subcritical pattern solutions (which correspond to a one-parameter continuum of periodic orbits) are reversible.

A general mechanism for the appearance of localized solutions in reversible dynamical systems has previously been proposed in [4–6]. On variation of a system parameter the two-dimensional unstable manifold of E_s [$W^u(E_s)$] will generically intersect the three dimensional collection of stable manifolds of P [$W^s(P)$] creating a heteroclinic connection between E_s and one of the periodic orbits P^0 of P (a front between the homogeneous and a pattern solution) [7]. Varying the parameter further leads to the intersection of $W^u(E_s)$ with Π in the region of the periodic solution. By reversibility, intersection of the unstable manifold of E_s with Π also implies intersection of the stable manifold of E_s [$W^s(E_s)$] with Π, and therefore an intersection of $W^u(E_s)$ and $W^s(E_s)$. The appearance of these intersections corresponds, therefore, to the birth of homoclinic solutions, biasymptotic to E_s, but passing close to the periodic solution P^0: the localized states. Analogous homoclinic connections of the periodic solutions are also implied, which resemble patterns containing holes [6, 4]. Varying the parameter still further leads to the eventual disappearance of localized states and fronts as the relevant manifolds cross the symmetry plane and eventually become disjoint once more. This scenario is depicted schematically in Fig. 13 of [4] and in Figs. 3 and 2 of [5] and [6] respectively, and elegantly explains the appearance and disappearance, through a sequence of saddle–node bifurcations, of localized states consisting of N adjacent peaks of the pattern, where N is a whole number. For our system (1), Fig. 1 shows the region of existence of DS with 1, 3 and 5 peaks in the I_s–θ parameter space, while Fig. 2 shows their bifurcation structure for a vertical cut of Fig. 1 at $\theta = 1.5$. As in [10] for the saturable absorber model, qualitatively this scenario is in agreement with the general theory outlined above [4–6].

This simple picture, however, considers only intersections between manifolds of the homogeneous solutions and manifolds of high-amplitude periodic patterns, i.e. only the existence of fronts between the homogeneous state and a pattern stable in the full PDE are assumed. Close to a degenerate Hamiltonian–Hopf bifurcation this is actually

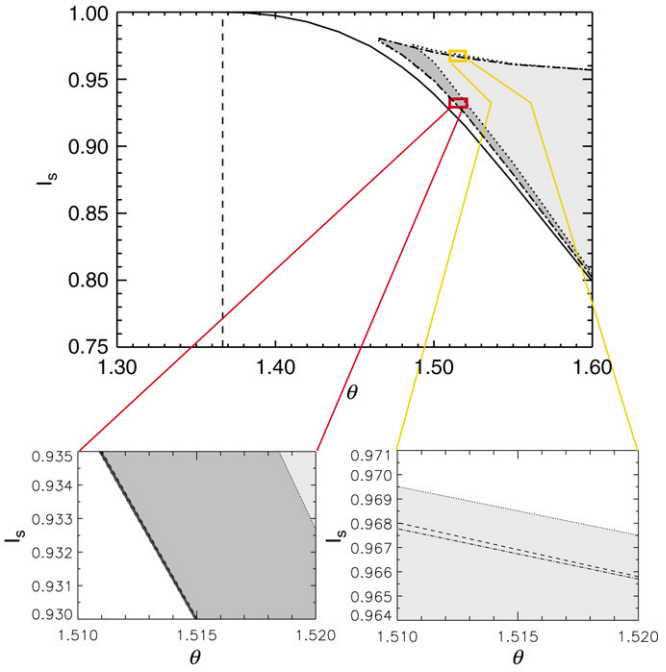

Fig. 1. Region of existence of DS in the two-dimensional I_s–θ parameter space. Dotted, dashed and dotted-dashed lines show the limits for localized structures with one, three and five peaks respectively. The solid line corresponds to the turning point (saddle-node) of a subcritical pattern with the critical wavenumber.

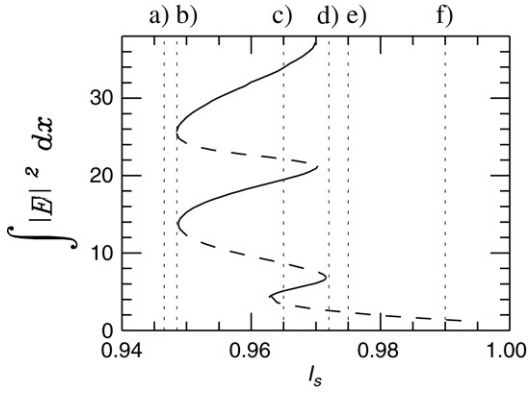

Fig. 2. Bifurcation structure of DS for $\theta = 1.5$. Solid (dashed) lines indicate stable (unstable solutions). From smaller to larger total intensity the solid lines correspond to localized structures with one, three and five peaks. The vertical dotted lines show the values of I_s in each panel of Fig. 3.

the case: low-amplitude periodic orbits (unstable patterns in the PDE) correspond to centre type periodic orbits of the dynamical system describing the stationary solutions of the PDE (their four Floquet multipliers lie on the unit circle) and, therefore, they have neither stable nor unstable manifolds [4]. As one moves away from the Hamiltonian–Hopf bifurcation point, however, some of these periodic orbits may acquire stable and unstable manifolds through a period doubling bifurcation by which two Floquet multipliers meet at -1 and move away from the unit circle on the real axis. In reversible systems, such period doubling bifurcations may induce very involved dynamics [11]. Moreover, these low-amplitude periodic solutions coexist with both high-amplitude periodic orbits and the homogeneous state in a whole parameter region, as the lower branches of subcritical bifurcations, and therefore the possibility of additional fronts connecting the homogeneous solution and low-amplitude patterns cannot be neglected. This modifies the structure of the phase space analyzed in [4–6] leading to new phenomena, including additional types of fronts and localized structures. This is actually the case in the systems studied here, and the exact nature of these structures, and the reason for their appearance, is the main subject of the rest of this paper.

To clarify what is actually occurring in (1), and possibly in other systems to which the analysis of [5,6] applies, we compute $W^u(E_s)$ and $W^s(P)$ and analyze the structure of the phase space in more detail. The four-dimensional vector field describing stationary solutions of Eq. (1) is given explicitly by:

$$\begin{aligned} d_x a &= \theta u + v - (u^2 + v^2)u \\ d_x b &= -u + \theta v - (u^2 + v^2)v + E_0 \\ d_x u &= a \\ d_x v &= b. \end{aligned} \tag{4}$$

To simplify the description we can follow the example of [4–6] and display trajectories on a Poincaré section $\mathcal{S}$ containing the symmetry plane Π. This will allow us to depict the intersections of the stable and unstable manifolds with each other, and with the symmetry plane, in a three dimensional space. Here we take the Poincaré section given by $a = 0$.

From the stability analysis of E_s one can parameterize $W^u(E_s)$ around the fixed point in the following way:

$$\begin{aligned} \delta u(\alpha,\phi) &= \alpha[u_s\cos(\phi+\psi) - v_s\cos(\phi)] \\ \delta v(\alpha,\phi) &= \alpha[u_s\cos(\phi) + v_s\cos(\phi+\psi)] \\ \delta a(\alpha,\phi) &= \alpha\{u_s[\mu\cos(\phi+\psi) - \nu\sin(\phi+\psi)] \\ &\quad - v_s[\mu\cos(\phi) - \nu\sin(\phi)]\} \\ \delta b(\alpha,\phi) &= \alpha\{u_s[\mu\cos(\phi) - \nu\sin(\phi)] + v_s[\mu\cos(\phi+\psi) \\ &\quad - \nu\sin(\phi+\psi)]\} \end{aligned} \tag{5}$$

where α and ϕ are the parameters, $\psi = \tan^{-1}(-\sqrt{1-I_s^2}/I_s)$, $\mu = \mathrm{Re}[\lambda]$ and $\nu = \mathrm{Im}[\lambda]$, where $\lambda = +\sqrt{\theta - 2I_s + i\sqrt{1-I_s^2}}$ is one of the eigenvalues of the fixed point with positive real part.

In order to generate the whole unstable manifold $W^u(E_s)$, we start from a family of initial conditions ($u_\phi = u_s + \delta u$, $v_\phi = v_s + \delta v$, $a_\phi = \delta a$, $b_\phi = \delta b$) with $0 \le \phi < 2\pi$ and $\alpha \ll 1$, and integrate Eqs. (4) forwards in x. The stable manifold $W^s(E_s)$ is the symmetrical image of $W^u(E_s)$ with respect to the symmetry plane Π given by $a = 0$ and $b = 0$.

We must also compute the unstable manifold $W^u(P^0)$ of the particular periodic orbit P^0 selected by the intersection of $W^s(E_s)$ and $W^u(P)$ (the "Pomeau" front). In order to generate $W^u(P^0)$ we must first know the wavelength of P^0. This is obtained from the numerical simulation of the full PDE for a large system, starting from an initial condition consisting of the homogeneous solution in one half of the spatial domain, and a periodic pattern of arbitrary wavelength in the other. During the evolution a front is formed and the

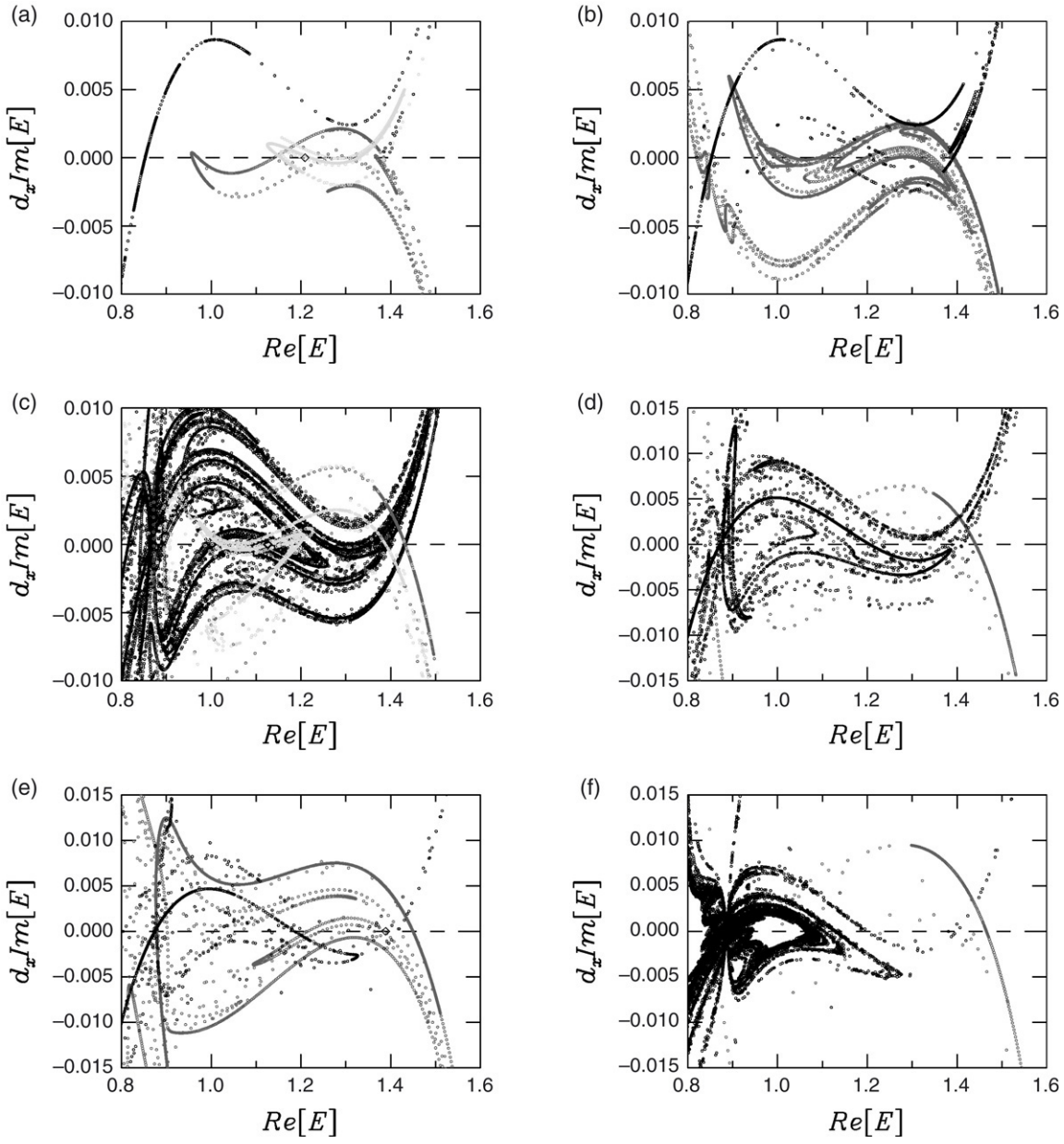

Fig. 3. Projection of the 3D Poincare section on the b–u plane for different values of the intensity I_s and $\theta = 1.5$. From top to bottom and left to right: $I_s = 0.946515$, 0.948504, 0.965, 0.972, 0.975 and 0.99. The black symbols belong to the stable manifold $W^s(E_s)$ of the fixed point E_s, and the dark grey ones to the unstable manifold $W^u(P^0)$ of the periodic orbit. In (a) the light grey symbols show the stable manifold $W^s(P_u)$ of the dynamically unstable pattern associated with P^0. In (b) grey symbols instead show the unstable manifold $W^u(P_u)$.

pattern region relaxes to the appropriate wavelength. Once we have determined its wavenumber we compute P^0 using a Newton method. The unstable direction in phase space can then be evaluated numerically: starting from a peak of the pattern, where P^0 crosses $\mathcal{S}$ on the symmetry plane Π, we integrate Eqs. (4) forwards in x until the trajectory crosses $\mathcal{S}$ again. Since the stable direction is contracting onto the periodic orbit, this indicates the unstable direction. We then discretize this segment between the two crossings with $\mathcal{S}$ into a number of points (typically of the order of several hundreds) and start a simulation from each such point. This generates a sufficient sample of the unstable manifold $W^u(P^0)$ of the periodic orbit P^0.

Fig. 3 shows $W^s(E_s)$ and $W^u(P^0)$ for increasing values of I_s, and $\theta = 1.5$. It is useful to compare the structure of the phase space shown in Fig. 3 with the bifurcation structure of cavity solitons for this value of the detuning shown in Fig. 2. We also note that the Re$[E]$ axis corresponds to the projection of the symmetry plane Π and, therefore, every intersection of a manifold with the horizontal axis is a projection of an actual intersection with Π, and so gives rise to a homoclinic orbit.

In Fig. 3(a) ($I_s = 0.946515$), where cavity solitons do not yet exist, $W^s(E_s)$ (black symbols) and $W^u(P^0)$ (dark grey symbols) do not intersect, indicating that a Pomeau front has not yet been formed. Note, however, that $W^u(P^0)$, the unstable manifold of the periodic orbit, already presents a high level of

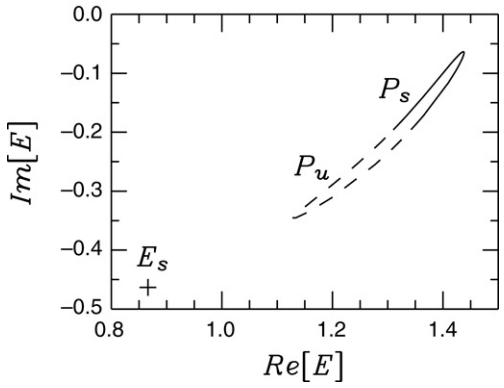

Fig. 4. Closed line formed by the set of stable and unstable periodic orbits, P_s and P_u, on the symmetry plane Π defined by $d_x\mathrm{Re}[E] = d_x\mathrm{Im}[E] = 0$. The cross indicates the homogeneous solution E_s.

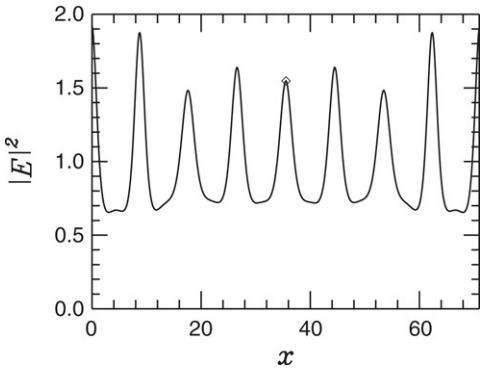

Fig. 5. Localized state consisting of a region of an unstable pattern within a stable one. This implies the existence of a front connecting both patterns. Here $\theta = 1.5$ and $I_s = 0.944$.

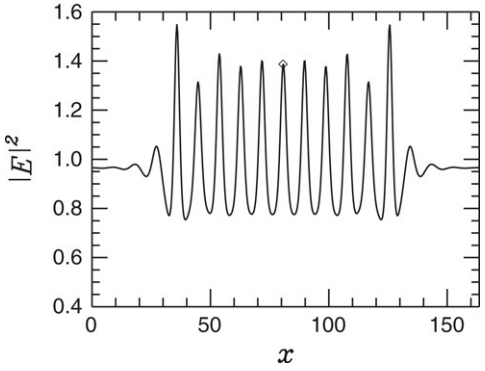

Fig. 6. Seven peaks localized structure associated with the unstable pattern. The central peak is very close to one oscillation of the unstable pattern. Here $\theta = 1.5$ and $I_s = 0.965$.

complexity. This stems from the topological structure of the one-parameter family of periodic orbits P. The intersection of this set of periodic orbits with the Poincaré section $\mathcal{S}$ forms a closed curve on the symmetry plane Π (Fig. 4). Fig. 4 has been obtained by plotting the intersection of pattern solutions of Eq. (1) with $\mathcal{S}$ ($d_x\mathrm{Re}[E] = 0$) for different values of their wavenumbers. Since periodic orbits are reversible, $d_x\mathrm{Im}[E]$ is also zero and these intersections lie on the symmetry plane. The pattern solutions are obtained as zeros of Eq. (1) by a Newton method where space has been discretized and periodic boundary conditions assumed. The line P is naturally divided in two portions P_u and P_s ($P = P_u \cup P_s$) corresponding to low and high-amplitude patterns [12]. These two subsets meet at the extreme values of the wavenumber in two folds. At these two points the four Floquet multipliers m of the periodic orbits take the value $m = +1$. Moving away from these points on P_s, i.e. changing the wavelength of the pattern, one Floquet multiplier moves along the real axis with $0 < m < 1$ and another with $1 < m$. Moving on P_u, however, all Floquet multipliers remain on the unit circle $|m| = 1$ but become complex. For parameter values far from the degenerate Hamiltonian–Hopf bifurcation analysed in [4], two of the Floquet multipliers may go all the way round the unit circle until $m = -1$, and collide leading to two Floquet multipliers on the real axis, one with $m < -1$ and another with $-1 < m < 0$.

In [5,6] only intersections of the Poincaré section $\mathcal{S}$ with the subset of periodic orbits P_s were considered and $\mathcal{S} \bigcap W^u(P)$ was assumed to be an open 2-dimensional surface. Instead, close to P, $W^u(P)$ is closed, and also very complicated. Moreover, the collection of unstable manifolds of the subset of periodic orbits P_s ($W^u(P_s)$) intersects the collection of stable manifolds of the other subset of periodic orbits P_u ($W^s(P_u)$, light grey symbols) creating heteroclinic intersections. By reversibility $W^u(P_s)$ also intersects $W^s(P_s)$ yielding homoclinic intersections. By the same argument as before, each crossing with the symmetry plane Π associated with these intersections creates additional homoclinic connections, i.e. localized states biasymptotic to a periodic orbit. Fig. 5 shows an example of such a localized state consisting of a region close to a low-amplitude pattern within a high-amplitude pattern. The symbol in the central peak indicates the crossing with the symmetry plane Π and it is also shown in Fig. 3(a). This indicates the existence of a "Pomeau" front between low and high-amplitude patterns. In this case, however, both sides of the front are members of one-parameter families and, therefore, the localized structures and the front itself belong to one-parameter families.

On increasing the control parameter, $W^s(E_s)$ and $W^u(P)$ intersect at some point between Fig. 3(a) and (b), selecting one of the orbits $P^0 \equiv P_s^0$ on the subset P_s. As the pump is increased (Fig. 3(c)) cavity solitons are created at each crossing of $W^s(E_s)$ with the symmetry plane Π in the predicted sequence. The complexity (fractal structure) of the heteroclinic connection, however, gives rise to an infinite number of other reversible homoclinic trajectories which correspond to different symmetric sequences in which DS can be arranged [6].

Due to the high level of complexity already present in $W^u(P)$, even before the heteroclinic intersection leading to the "Pomeau" front between the homogeneous and high-amplitude pattern solutions takes place, $W^s(E_s)$ has an even higher level of complexity than described in the previous paragraphs and in [4–6]. In particular, $W^s(E_s)$ has a region of high complexity in the neighbourhood of the low-amplitude patterns P_u. Fig. 3(c) depicts $W^u(P_u^0)$, where P_u^0 denotes the low-amplitude pattern with the same wavenumber as P^0, in light grey symbols for comparison, and indicates, approximately, the intersection of this manifold with $W^s(E_s)$. This shows

that extra fronts associated with the low-amplitude pattern exist, accompanied by a whole set of localized structures, analogous to those associated with the stable pattern. Fig. 6 shows an eleven-peak DS arising from the low-amplitude pattern, i.e. it is a homoclinic trajectory biasymptotic to the homogeneous solution but passing very close to the low-amplitude patterns. The side peaks have the height of DS associated with the high-amplitude pattern, indicating that this homoclinic trajectory, before going close to the low-amplitude pattern, passes through the vicinity of the high-amplitude ones. The symbol at the maximum of the central peak indicates the intersection with the symmetry plane, and is also shown in Fig. 3(c). In the dynamical system (4) these solutions appear as stable–unstable pairs, but their precise bifurcation structure is not described by the general theory presented above and will be reported elsewhere. In the PDE (1), since the underlying pattern is dynamically unstable, such localized solutions are also unstable.

On further increasing the control parameter one starts to encounter the sequence of saddle–node bifurcations which destroy the localized solutions at the other end of the pinning region in parameter space (Fig. 2), until eventually the last single peak DS disappears. This occurs just before the situation depicted in Fig. 3(d). Before this point, however, $W^s(E_s)$ and $W^u(P)$ should have become disjoint [5,6], with the disappearance of the front between the stable pattern and homogeneous solutions. The latter is actually the case, but $W^s(E_s)$ and $W^u(P^0)$ still seem to intersect. We believe this is due to the existence of at least one N-heteroclinic intersection that goes to the high-amplitude pattern only after one or more orbits close to the, originally, only remaining single peak DS (which in the PDE correspond to the unstable DS). Associated with such a front would be a set of N-homoclinic trajectories (with $N > 1$) not described in [4,5], where only 1-homoclinic trajectories were studied. An example of such a localized state is shown in Fig. 7 [13]. It consists of three peaks; the two at the sides have an amplitude corresponding to the "pde-unstable" DS, while the one in the middle has a height similar to previous "pde-stable" DS. The symbol in the central peak of Fig. 7 indicates the intersection with the symmetry plane. Note its vicinity to the high-amplitude pattern solutions in Fig. 3(e) where this intersection is shown with the same symbol. We recall that for these parameter values there are no stable DS. Even for values of the control parameter far from the limits of stable DS existence $W^s(E_s)$ and $W^u(P_s)$, and $W^s(E_s)$ and Π, still intersect (Fig. 3(f)). We also note that for these values of the control parameter the heteroclinic connection between the homogeneous and low-amplitude pattern solution has been destroyed. In this case, this is due to the disappearance of the manifolds of the periodic orbit, again via an inverted period doubling bifurcation by which two Floquet multipliers collide at -1 and remain on the unit circle with opposite imaginary part. The absence of manifolds can be appreciated in Fig. 3(f) as a hole in the unstable manifold of the fixed point in the region close to the unstable pattern ($\mathrm{Re}[E] \simeq 1$).

All these new localized states and fronts not considered in previous analyses are most likely unstable since they involve

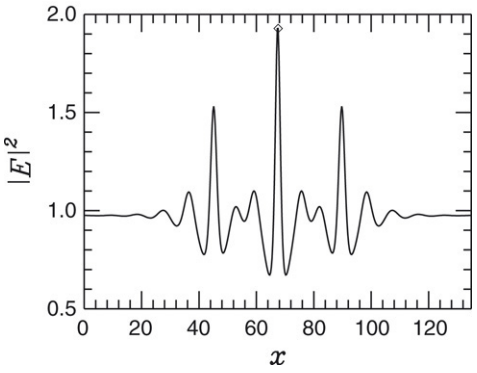

Fig. 7. Unusual DS in a parameter region where DS are not supposed to exist ($\theta = 1.5$ and $I_s = 0.972$). The central peak corresponds to a stable pattern, and the two outer peaks are unstable DS.

unstable solutions of the underlying PDE's. This is not always the case as in some particular situations the composition of unstable solutions may lead to stable structures [15]. In the present system, however, we have explicitly checked some such solutions and confirmed that they are unstable. In any case, a precise knowledge of the phase space, including dynamically unstable solutions, is crucial for the understanding of the dynamics of the system as a whole. For example, in this system with two transverse dimensions DS exhibit an excitable regime where unstable DS play a crucial role in the dynamics [16].

3. Saturable absorber in an optical cavity

In order to demonstrate that the results shown in the previous section are general and do not depend on specific features of the model, we have studied the structure of the phase space in a different system: a cavity filled with a saturable absorber [3,17,18]

$$\partial_t E = -(1 + \mathrm{i}\theta)E + \mathrm{i}\partial_x^2 E + E_0 - \frac{2C}{1 + |E|^2}E, \tag{6}$$

where E is the slowly varying amplitude of the electromagnetic field, θ is the cavity detuning, C is the scaled atomic density parameterizing both linear and nonlinear absorption, E_0 is the amplitude of the external field, and $\mathrm{i}\partial_x^2$ models diffraction. In Ref. [10] the existence and stability properties of DS were determined for this system. As in the Kerr cavity model the bifurcation structure of DS is qualitatively in agreement with the scenario proposed in [4–6].

Like the Kerr cavity, however, the phase space shows a much higher degree of complexity than previously assumed. Fig. 8 shows $W^s(E_s)$ and $W^u(P)$ for $\theta = -1$ and different values of the input pump E_0 (cf. Fig. 3 for the Kerr cavity). For this value of the detuning the unpinning transitions of the stationary front between the homogeneous solution and the dynamically stable periodic pattern take place at $I_s \simeq 1.065$ and $I_s \simeq 1.465$. The stable and unstable manifolds of the fixed point and periodic orbits show the same qualitative features discussed in the previous section. Before the heteroclinic connection is formed, the unstable manifold of the high-amplitude periodic orbit already shows a heteroclinic connection with the low-amplitude one, as well as a homoclinic intersection with the

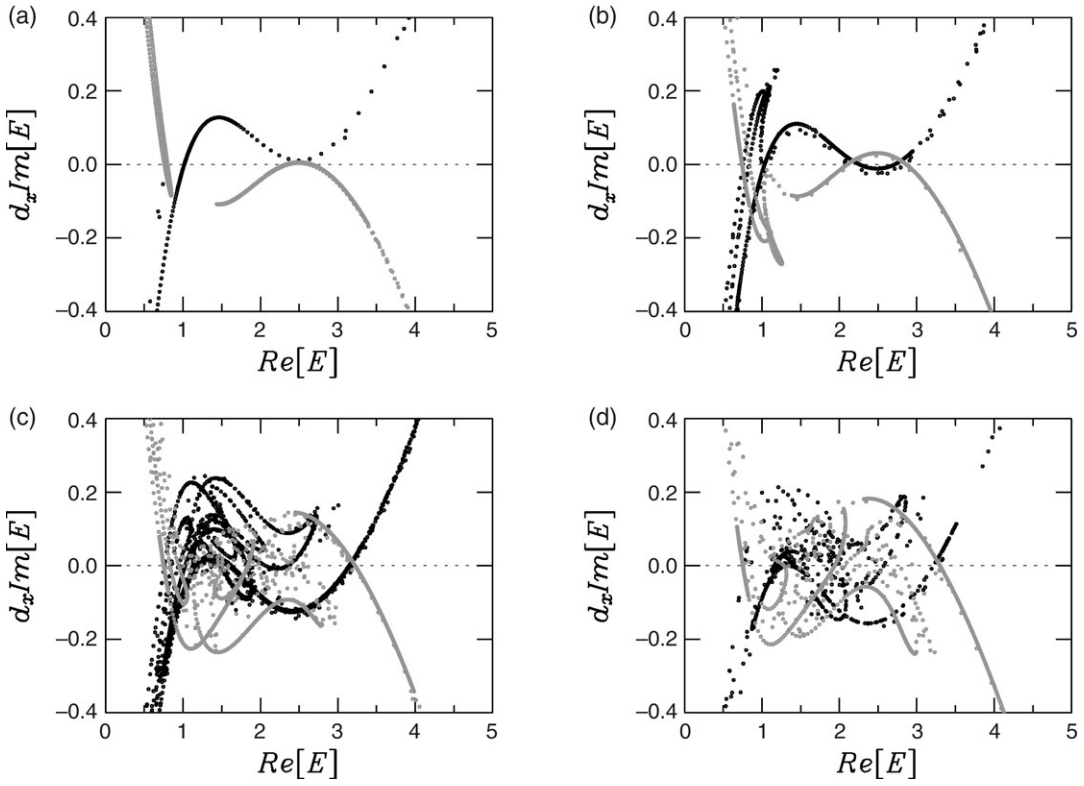

Fig. 8. The same as in Fig. 3, but for the saturable absorber model (Eq. (6)). Here $\theta = -1.0$ and, from top to bottom and left to right, $Is = 1.06$, 1.1, 1.4, and 1.6.

stable manifold (Fig. 8(a)). On increasing the control parameter DS are created at each crossing of $W^s(E_s)$ with the symmetry plane Π in the predicted sequence [10] (Fig. 8(b)), but soon much more complexity arises from the heteroclinic intersection of $W^s(E_s)$ with the unstable manifold of the low-amplitude periodic patterns (Fig. 8(c)). Finally, as in the previous case, this complexity remains far beyond the unpinning transition of the "Pomeau" front (Fig. 8(d)).

4. Conclusions

We have presented a numerical analysis of the four dimensional reversible dynamical system describing stationary solutions of an optical cavity filled with a self-focusing Kerr medium. Comparing the structure of its phase space with the one predicted by the general theory described in [4–6], we have found a much higher level of complexity than expected. This complexity arises from the fact that the low-amplitude patterns that form part of the closed one-parameter family of periodic orbits have stable and unstable manifolds that intersect both invariant manifolds of the homogeneous and high-amplitude pattern solutions. As a result new fronts and localized solutions exist. In particular, we have reported on new localized states associated with heteroclinic connections between (i) low and high-amplitude patterns, (ii) homogeneous solution and low-amplitude patterns, and (iii) homogeneous solution and high-amplitude patterns via the pde-unstable DS. Even if these new localized structures are unstable in the PDE, knowing the global structure of the phase space is crucial for the understanding of the dynamics of the system. Therefore, we conclude that the theory based on generic properties of reversible dynamical systems proposed in [4–6], and valid only close to a degenerate Hamiltonian–Hopf bifurcation, needs to be generalized away from that point to include the role of the low-amplitude patterns in shaping the phase space.

Acknowledgements

We thank A.R. Champneys and T. Wagenknecht for useful discussions. We acknowledge financial support from FunFACS and EPSRC (Grant No. GR/S28600/01).

References

[1] P. Umbanhowar, F. Melo, H.L. Swinney, Nature (London) 382 (1996) 793;
O. Thual, S. Fauve, J. Phys. (Paris) 49 (1988) 1829;
J.E. Pearson, Science 261 (1993) 189;
K.J. Lee, et al., Science 261 (1993) 192;
I. Müller, E. Ammelt, H.G. Purwins, Phys. Rev. Lett. 82 (1999) 3428.
[2] W.J. Firth, C.O. Weiss, Opt. Phot. News 13 (2002) 55;
L.A. Lugiato (Ed.), Feature Section on Cavity Solitons, IEEE J. Quant. Elect. 39 (2) (2003);
M. Tlidi, P. Mandel, R. Lefever, Phys. Rev. Lett. 73 (1994) 640;
B. Schäpers, et al., Phys. Rev. Lett. 85 (2000) 748;
S. Barland, et al., Nature 419 (2002) 699.
[3] W.J. Firth, A.J. Scroggie, Phys. Rev. Lett. 76 (1996) 1623.
[4] P.D. Woods, A.R. Champneys, Physica D 129 (1999) 147.
[5] P. Coullet, C. Riera, C. Tresser, Phys. Rev. Lett. 84 (2000) 3069.
[6] P. Coullet, C. Riera, C. Tresser, Chaos 14 (2004) 193.
[7] Y. Pomeau, Physica D 23 (1986) 3.
[8] L.A. Lugiato, R. Lefever, Phys. Rev. Lett. 58 (1987) 2209.
[9] A.J. Scroggie, et al., Chaos Solitons Fractals 4 (1994) 1323.
[10] J.M. McSloy, et al., Phys. Rev. E 66 (2002) 046606.
[11] A. Vanderbauwhede, SIAM J. Math. Anal. 21 (1990) 954.

[12] Sub-scripts u (s) in P stand for unstable (stable) in the PDE.
[13] We cannot completely discard the possibility that such a structure is not due to the existence of the proposed N-heteroclinic orbits, but is associated with the 1-homoclinic orbits discussed earlier. In that case, the existence of the N-heteroclinic orbits would remain an open question [14].
[14] J. Härterich, Physica D 112 (1998) 187.
[15] C.K.R.T. Jones, M. Romeo, Phys. Rev. E 63 (2001) 011904; B. Sandstede, A. Scheel, Nonlinearity 13 (2000) 1465.
[16] D. Gomila, M.A. Matías, P. Colet, Phys. Rev. Lett. 94 (2005) 063905.
[17] G.K. Harkness, W.J. Firth, G.-L. Oppo, J.M. McSloy, Phys. Rev. A 66 (2002) 046605.
[18] L.A. Lugiato, C. Oldano, Phys. Rev. A 37 (1988) 3896.